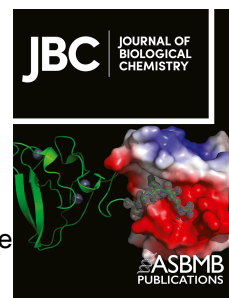


Journal Pre-proof

$\alpha\beta$ T cell receptor recognition of self-phosphatidylinositol presented by CD1b

Rachel Farquhar, Ildiko Van Rhijn, D. Branch Moody, Jamie Rossjohn, Adam Shahine



PII: S0021-9258(22)01292-3

DOI: <https://doi.org/10.1016/j.jbc.2022.102849>

Reference: JBC 102849

To appear in: *Journal of Biological Chemistry*

Received Date: 6 September 2022

Revised Date: 21 December 2022

Accepted Date: 23 December 2022

Please cite this article as: Farquhar R, Van Rhijn I, Moody DB, Rossjohn J, Shahine A, $\alpha\beta$ T cell receptor recognition of self-phosphatidylinositol presented by CD1b, *Journal of Biological Chemistry* (2023), doi: <https://doi.org/10.1016/j.jbc.2022.102849>.

This is a PDF file of an article that has undergone enhancements after acceptance, such as the addition of a cover page and metadata, and formatting for readability, but it is not yet the definitive version of record. This version will undergo additional copyediting, typesetting and review before it is published in its final form, but we are providing this version to give early visibility of the article. Please note that, during the production process, errors may be discovered which could affect the content, and all legal disclaimers that apply to the journal pertain.

© 2022 THE AUTHORS. Published by Elsevier Inc on behalf of American Society for Biochemistry and Molecular Biology.

$\alpha\beta$ T cell receptor recognition of self-phosphatidylinositol presented by CD1b

Rachel Farquhar¹, Ildiko Van Rhijn^{2,3}, D. Branch Moody², Jamie Rossjohn^{1,4*}, Adam Shahine^{1*}.

¹Infection and Immunity Program and Department of Biochemistry and Molecular Biology, Biomedicine Discovery Institute, Monash University, Clayton, Victoria, Australia. ²Division of Rheumatology, Inflammation, and Immunity, Brigham and Women's Hospital and Harvard Medical School, Boston, Massachusetts, USA. ³Department of Infectious Diseases and Immunology, Faculty of Veterinary Medicine, Utrecht University, Utrecht, the Netherlands. ⁴Institute of Infection and Immunity, Cardiff University, School of Medicine, Cardiff, United Kingdom

* **Joint senior and corresponding authors:** Adam Shahine: adam.shahine@monash.edu;
Jamie Rossjohn: jamie.rossjohn@monash.edu

Running title: TCR recognition of CD1b presenting PI

Keywords: antigen presentation; autoreactivity; glycolipid; phospholipid; X-ray crystallography, T cell receptor (TCR); CD1b

ABSTRACT

CD1 glycoproteins present lipid-based antigens to T cell receptors (TCRs). A role for CD1b in T cell-mediated autoreactivity was proposed when it was established that CD1b can present self-phospholipids with short alkyl chains (~C34) to T cells; however, the structural characteristics of this presentation and recognition are unclear. Here we report the 1.9 Å-resolution binary crystal structure of CD1b presenting a self-phosphatidylinositol-C34:1 (PI) and an endogenous scaffold lipid. Moreover, we also determined the 2.4 Å structure of CD1b-PI complexed to an autoreactive $\alpha\beta$ TCR, BC8B. We show the TCR docks above CD1b and directly contacts the presented antigen, selecting for both the phosphoinositol headgroup and glycerol neck region via antigen remodelling within CD1b and allowing lateral escape of the inositol moiety through a channel formed by the TCR α -chain. Furthermore, through alanine scanning mutagenesis and surface plasmon resonance, we identified key CD1b residues mediating this interaction, with Glu-80 abolishing TCR binding. We additionally define a role for both CD1b $\alpha 1$ and $\alpha 2$ molecular domains in modulating this interaction. These findings suggest the BC8B TCR contacts both the presented phospholipid and the endogenous scaffold lipid via a dual mechanism of co-recognition. Taken together, these data expand our understanding into the molecular mechanisms of CD1b-mediated T cell autoreactivity.

INTRODUCTION

While peptide antigen recognition forms the central dogma of classical T cell mediated adaptive immunity, the role of lipids as non-classical antigens, presented by MHC class I like molecules known as

CD1, are emerging as new targets of protective and autoimmunity. CD1 mediated T cell response to bacteria like *Mycobacterium tuberculosis* (*Mtb*) (1-14), and self-lipid antigens mediate autoreactivity and autoimmune disease via lipid activation (15, 18, 24-27), lipid - independent binding (16, 19, 21-23), and lipid blocking mechanisms (20).

While mice only express CD1d, humans express CD1a, CD1b, CD1c, CD1d and CD1e, which differ based on function, tissue localisation, and sequence (28, 29). The mechanisms of antigen presentation by CD1d and recognition by Natural Killer T cell receptors (NKT TCRs) are well established and involve direct TCR contact with the protruding headgroup moiety (17, 31-33). However, emerging research has revealed recognition events that include mechanisms of direct CD1 protein recognition without recognition of carried lipid, cross reactivity of many antigens based on their neck regions, and sideways approaches of TCRs to CD1 proteins (10, 22, 23, 26, 27, 34).

CD1b exhibits the largest antigen binding cleft among isoforms in the CD1 family, which allows the molecule to accommodate a range of foreign- and self-lipid antigens with aliphatic hydrocarbon tails of up to C80 in length (10, 12, 26, 27, 35, 36). In some cases, a scaffold lipid is simultaneously bound inside CD1b along with the recognized antigen to stabilise its internal architecture (36-38). CD1b presents very long chain foreign mycolyl lipids (39, 40) to germline encoded mycolyl-reactive (GEM) and LDN5 like TCRs (10, 11, 41), with conserved TCR genes. (42). Additionally, CD1b presents self-lipid antigens, either cellular phospholipids or sphingolipids, to autoreactive $\alpha\beta$ and $\gamma\delta$ T cells (25-27).

Myeloid DCs (43) can regulate CD1b expression and activate CD1b-restricted T cells, inducing an autoreactive immune response (28, 44). Further, the presentation of self-phospholipid antigens by CD1b is possibly linked to oxidative stress in the case of phosphatidylglycerol (PG) presentation (27, 45), as well as playing a role in both hyperlipidaemia and protection against CD1b+ T cell lymphoma mediated by presentation of phosphatidylethanolamine (PE) (46, 47).

To date, three CD1b-lipid antigen-TCR crystal structures have been solved, (10, 26, 27). The mechanism of germline encoded mycolyl reactive (GEM) $\alpha\beta$ TCR, GEM42, in recognition of CD1b presenting glucose 6-monomycolate (GMM) emphasizes how an invariant TCR contacts the protruding glycan epitope (48, 49). Other autoreactive T cells display diverse patterns of TCR expression and molecular modes of recognition of CD1b-lipid complexes (26, 27, 45).

An emerging classification system divides CD1b-TCR interactions into three categories: TCRs are highly specific for individual lipid structures, broadly reactive to a family of structurally related lipids or CD1b-specific in a lipid independent manner (26). For example, structural determination of CD1b in complex with autoreactive TCR PG90 (TRAV26-1/TRBV7-8) was highly specific for the phospholipid bound, whereas BC8B (TRAV9-2/TRBV6-2) could respond broadly to many glycerylphospholipids. This promiscuous recognition occurs because the TCR binds the neck region that is common to many phospholipid classes (26, 27). In both cases, the TCR directly recognised the amphipathic lipid headgroups exposed on the outer surface of CD1b, but not the scaffold lipid, which is typically seated

beneath the antigenic lipid, distant from the TCR.

With only three solved ternary structures, our understanding of CD1b antigen recognition is in its early phase. To further understand the molecular mechanisms underpinning CD1b-self lipid antigen recognition, we sought to solve the structure of CD1b presenting a self-glycophospholipid in complex with an autoreactive $\alpha\beta$ TCR, BC8B. We determined the crystal structures of CD1b presenting self-phosphatidylinositol (CD1b-PI-C34:1) and CD1b-PI-C34:1-BC8B TCR, and conducted alanine scanning mutagenesis on CD1b surface residues involved in BC8B TCR docking evaluated via surface plasmon resonance. Our findings support the model of broadly reactive $\alpha\beta$ TCR recognition of CD1b presenting self-antigens, highlight conserved residues necessary for CD1b-phospholipid recognition by BC8B, and provide direct evidence of dual recognition directed towards both the presented antigen and the scaffold lipid.

RESULTS

Molecular mechanisms of CD1b presentation of cellular PI

Previous structural determination of the molecular mechanisms of PI-C33:0 presentation by CD1b involved the refolding of CD1b expressed in *Escherichia coli*, which included the determination of artificially loaded detergent molecules within the binding pocket (36). In this study, we sought to determine the structure of CD1b exogenously loaded with cellular PI that contains two alkyl chains, C18 and C16:1, which combined have an overall unsaturation profile of C34:1. Cellular endogenous lipids were displaced from CD1b by first loading with lysosulfatide, and subsequently loaded with PI, and purified via anion exchange

chromatography (**Figure 1A**). Lipid loaded onto CD1b was validated by isoelectric focusing gel (IEF) (**Figure 1B**), before being crystallised and the structure of CD1b-PI solved to a resolution of 1.9 Å (**Figure 2A, Table 1**). The electron density for both PI acyl tails were clearly defined, with the C18:1 sn2 tail extending towards the base of the A' portal, and the C16:0 sn1 tail anchored in the C' portal (**Figure 2B**). In addition, a single tube of electron density was observable with the T' and F' portals, corresponding to a single scaffold lipid 31 carbons in length, where the lipid remains buried within the F' pocket (**Figure 2B**).

The CD1b-β2m complex reported here was expressed in human embryonic kidney (HEK) 293S cells and exogenously loaded with PI-C34:1. This structure shares many similarities with the previously determined refolded CD1b-PI (PI-C33:0) structure (36), which overlay with a root mean square division (R.M.S.D) of 0.53Å. Positioning of acyl tails and phosphate headgroup are highly similar across both structures. However due to sn1 tail length differences by 1 carbon, PI-C33:0 penetrates deeper into the C' portal. The CD1b α2 hinge region bends towards the PI-C34:1 headgroup, where the inositol moiety is anchored by via hydrogen bond. This isn't the case with PI-C33:0 (**Figure 2C**), where the side chain of Gln152 faces in the opposite direction, away from PI-C33:0. This interaction between inositol and the outer surface of CD1b is notable because previously determined CD1b-phospholipid antigen structures show no significant contacts made between CD1b and the solvent exposed headgroup (38).

The key differences between the positioning of CD1b-PI-34:1 and CD1b-PI-C33:0 relates to the endogenous scaffold and detergent molecules positioned within the F' portal. The F' portal, which provides

access of the antigen to the outer surface of CD1b, is capped by a van der Waals (VDW) network among Glu80, Phe84, and Tyr151. The endogenous scaffold lipid is buried underneath the F' portal with the VDW network remaining intact. In the previously observed structure detergent molecules disrupt the opening of the F' portal, with Tyr151 being displaced and rotated towards the solvent (**Figure 2D**) (36). However, as the positioning of Tyr151 plays a role in TCR recognition (26), where dual the spacer lipid and presented lipid is required for TCR contact, the movement of the positioning of Tyr151 appears to be dependent upon scaffold lipid length. Extension of the scaffold lipid to the outer surface of CD1b is unusual, as it normally lies beneath and beside, rather than above the antigenic lipid.

BC8B TCR docking onto CD1b-PI-C34:1

To ascertain the molecular mechanisms of CD1b-PI recognition, we produced the BC8B TCR and co-crystallised with CD1b-PI, with the ternary structure determined to a resolution of 2.4 Å (**Figure 3A, Table 1**). There is incomplete density for the solvent exposed inositol ring and well-defined density for the phosphate moiety (**Figure 3B**). Clear tubes of density are present for the sn1 and sn2 acyl tails and spacer lipid. Compared with the previously solved structure of unliganded BC8B (PDB ID: 6CUH) (26), we observe negligible remodelling of the BC8B TCR upon docking onto CD1b-PI-C34:1, where unliganded and complexed TCRs overlay with an overall R.M.S.D of 0.88Å. However PI-C34:1 is lifted out of the antigen binding pocket by the CDR1α and CDR3α loops of the variable domain of the BC8B TCR (BC8B-Vα), resulting in an upward shift of the entire lipid by 4Å (**Figure 3C**).

The CDR1α and CDR3α regions specifically contact the sn1 acyl tail in the C' portal and

the phosphate neck region, which connects the glyceryl unit to the inositol ring. The inositol moiety protrudes furthest from CD1b but instead of contacting the TCR, escapes laterally through a TCR escape channel formed between by CDR1 α and CDR3 α loops and situated above the A' roof of CD1b (**Figure 4A-B**). Thr28 α and Gln113 α stack against the inositol moiety and, as well as above by framework residue Asn2 α , where they partially angle the inositol for escape. Whilst not part of the lateral escape channel, additional hydrogen bonds are formed with the phosphate and glycerol moieties by Ser107 α and Tyr114 α respectively, which lock in place the features shared across all phospholipid species (**Figure 4A**).

The lateral escape channel was previously observed in the context of phosphatidylcholine (PC) recognition (26). This CD1b-PC-TCR example was proposed as a candidate mechanism by which TCRs could broadly recognize phospholipids, if the class defining head group that is distal to the phosphate moiety escapes from the TCR-CD1 interface. However, evidence for escape of more than one headgroup was lacking, and it was unknown whether a larger phospholipid headgroup such as inositol in PI, would be recognised. For example TCR docking might be hindered or enhanced by steric or electrostatic interactions with the inositol ring in PI. Here CDR3 α is more involved in recognition of PI compared to PC, with additional hydrogen bonds formed with Ser107 α and Tyr114 α against the phosphate and neck regions respectively. Further, due to the larger size of the inositol moiety compared to choline, the TCR α -chain framework (FW) and CDR1 α partially contact the inositol via VDW interactions, which in turn angle the headgroup to escape through the channel (**Figure 4A**).

Interaction between CD1b and BC8B TCR is primarily mediated by the CDR3 β region, which anchors the TCR above the F' pocket (**Figure 4C-D, Supplemental Table 1**). Recognition of CD1b is largely mediated via a network of polar contacts formed between CD1b α 1 localised residues (Arg79, Glu80, Asp83, and Asp87), and BC8B TCR CDR3 α - β (**Figure 4C**). Where BC8B-V β forms a complex network of interactions with CD1b α 1 domain with comparatively minor BC8B-V α engagement, BC8B-V α forms the majority of the contacts with the presented lipid via the CDR1 α and CDR3 α loops (**Figure 4A**). This indicates that the two TCR chains have distinct yet harmonious roles in the recognition of CD1b-lipid complex: BC8B-V β anchors onto CD1b whereas BC8B-V α determines phospholipid binding.

BC8B TCR recognises the diacylated phospholipid in a nearly identical manner when compared to CD1b-PI-BC8B and CD1b-PC-BC8B (**Figure 4B**). This was as expected due to the similarities in previously observed steady state affinity measurements between CD1b-PC and CD1b-PI contacted by BC8B (26). Structurally, both lipids are presented in a near identical manner, with both phospho-headgroup moieties overlaying closely. Furthermore, the lateral escape channel formed between the CDR1 α and CDR3 α regions is conserved, with a distance of 9.1 Å between Thr28 α and Thr113 α (**Figure 4B**) (26). Overall, these support the head group model by showing how two different head groups can escape.

Dual antigenic PI-C34:1 and scaffold lipid contact by BC8B TCR Leu111 β

Comparing TCR liganded and non-TCR liganded structures, Leu111 β displaces Tyr151 on CD1b, resulting in a 90° rotation of its sidechain (**Figure 4D**). This rotation is

observable in the presence of higher placed spacer lipids that move up within the F' portal, as compared to the previous CD1b-PI C33:0 binary structure. This rotation is also observed within the complex of BC8B-CD1b-PC, however the scaffold lipid observed in the previously determined crystal structure was shorter (26), and as such, TCR contact was not observed.

Prior crystallographic data have demonstrated that CD1b-restricted TCRs specifically bind the antigenic lipid, while 'ignoring' the buried scaffold lipid. Here, the CDR3 β region tightly locks onto CD1b above the F' pocket, via a network of polar contacts (**Figure 4C**). This mode of contact allows Leu111 β of CDR3 β to penetrate the F' portal, where it contacts both the sn1 antigenic acyl tail at the entrance to the C' portal, and the terminus of the C31 scaffold lipid at the F' portal opening.

This similar mechanism is observed in the previously determined complex of BC8B-CD1b-PC, however the scaffold lipid does not protrude high enough out of the F' portal to permit contacts with Leu111 β (**Supplementary Figure 1A-B**) (26). In comparison, Leu110 β of the GEM42 TCR again penetrates the F' pocket of CD1b upon GMM presentation, but favours contacts with the internal CD1b residue Phe84 (**Supplementary Figure 1C**) (10). A similar mechanism is observable for the CDR3 α Leu99 α residue of the human CD1d reactive NKT15 iNKT TCR, both of which do not involve dual lipid contacts (**Supplementary Figure 1D**) (17). Thus, unlike other CD1-reactive TCRs, hydrophobic bond-mediated dual recognition of the antigenic-scaffold and the TCR CDR3 β is observed (**Figure 4D**).

Energetic footprint reveals conserved role for Glu80 in TCR recognition

Alanine scanning mutagenesis was carried out to determine the impact of CD1b amino acid residues on BC8B TCR recognition. Specifically, we sought to determine the importance of contacts conserved across both CD1b-lipid-BC8B TCR structures. Based on contacts with the BC8B TCR, eight CD1b-mutants containing endogenous lipids were produced, and steady state binding kinetics towards BC8B TCR were analysed via surface plasmon resonance (SPR) (**Figure 5A**).

The BC8B TCR exhibits a steady state affinity of 13.6 μ M for untreated CD1b-Wild Type (WT) that is loaded with a mixture of endogenous (endo) cellular lipids sourced from the expression system. Previous SPR analysis determined that the BC8B TCR binds CD1b-endo and CD1b-PI with a similar affinity of 9.3 μ M and 9.7 μ M respectively (26). This outcome can be explained by the high content of phospholipids in endogenous CD1b and the ability of the TCR to cross recognize many phospholipid classes (27). As such, SPR analysis was conducted using CD1b-endo mutants for all affinity measurements. In this analysis, we found that none of the individual CD1b mutants enhanced BC8B TCR binding affinity compared to CD1b-WT. A change in affinity of CD1b-BC8B TCR was considered negligible if no fold change in steady state affinity was observed (Gln152, Glu156), moderate if ≤ 3 -fold reduction occurred (Arg79, Tyr151), significant if 3-5-fold reduction (Val72, Asp83) occurred, and critical if ≥ 5 -fold reduction occurred or abolishment of binding was seen (Glu80, Ile154) (**Figure 5A-B**).

Tyr30 α of the TCR is wedged between CD1b residues Gln152 and Glu156 via VDW interactions; however, abolishment of these CD1b residues have no significant impact on BC8B TCR affinity (**Figure 5C**).

Arg79 forms hydrogen bonds with Pro109 β of the CDR3 β , and Tyr112 α of the CDR3 α (**Figure 5D**). Leu111 β displaces Tyr151 via VDW interactions, allowing for CDR3 β to penetrate the F' portal opening (**Figure 5C**). A less than 3-fold reduction in binding was observed for Arg79Ala and Tyr151Ala, signifying moderate impact of this interaction of CD1b-BC8B binding. A 3-5 fold reduction in binding affinity was recorded for Val72Ala and Asp83Ala on the α 1 helix. Val72 and Asp83 form VDW and salt bridge interactions with Tyr112 α on CDR3 α and Arg112 on CDR3 β , respectively, with Val72 contributing to the correct formation of the C' portal (**Figure 5D**). This suggests significant impact due to both altering contacts with the key anchoring residue Arg112 β , and correct formation of the C' portal for correct lipid presentation, respectively.

Glu80Ala and Ile154Ala on the α 1 and α 2 helices respectively recorded a greater than 3-5-fold reduction in affinity. Whilst not forming key contacts with the BC8B TCR, Ile154 plays a critical role in antigenic lipid anchoring by forming the architecture of the CD1b C' portal, which is a CD1b-specific structure located beneath the α -helix, and is thought to allow escape of long lipids (36). Ile154 stacks against the sn2 acyl tail of PI, which anchors the presented antigen to allow for correct recognition by the BC8B TCR (**Figure 5C**). These data show that anchoring and recognition of CD1b by the BC8B TCR is mediated via the α 1 helix of CD1b and the BC8B-v β interface. Glu80 forms a network of VDW and polar contacts with Leu111 and Arg110 of CDR3 β , and we found that alanine mutation of these residues abolished BC8B binding (**Figure 5D**). This finding is consistent with previous CD1b-mutant studies where CD1b-lipid recognition is reduced or abolished by the Glu80Ala mutant in $\alpha\beta$ TCRs GEM42, PG90,

and PG10 (27). This is due to the conserved role of Glu80 in hydrogen bond mediated contact with the TCR-v β (10, 26, 27), and its role in forming the F' portal opening. Taken together, through structural and functional analysis, it has been determined that residues on the surface of α 1 domain of CD1b play a greater role than that of the α 2 domain, with a denser cluster of residues with a critical or significant role in the binding of CD1b-BC8 TCR compared to previously characterised complexes with the GEM42 and PG90 TCRs (16, 27).

Defining the interface of BC8B TCR-CD1b and subsequent lipid headgroup mediation

This is the fourth CD1b-TCR ternary structure determined to date (10, 26, 27), advancing our understanding of the mechanisms governing lipid head group recognition by a CD1b-reactive TCRs. In all four cases, the $\alpha\beta$ TCR shows a small incident angle with CD1b to generate somewhat similar footprints on the distal surface CD1b in contrast with the recently observed $\gamma\delta$ TCRs that fail to recognize carried antigen due to their sideways binding to CD1a (16) and possibly CD1b (25). Whereas all four examples now increasingly point to TCR approach to the membrane distal surface of CD1b, the data can also distinguish between and explain the differing mechanisms of broadly reactive and antigen specific CD1b restricted TCRs (**Figure 6A-B**). In each case, TCR binding towards CD1b is dependent on direct contact and recognition of the antigenic lipid being presented (**Figure 6C**). Further, the newly determined BC8B TCR-CD1b-PI structure validates the broad model of antigenic recognition as hypothesised with the BC8B-CD1b-PC-structure. Here, the TCR directly contact the phosphate, glycerol, and sn1 acyl tail. These chemical elements can be considered common to the 'neck' region of

PI and PC, as well as many other common diacylated phospholipids, but are lacking in lysolipid and sphingolipid antigens. In contrast with this promiscuous mechanism of response to many types of phospholipids, other antigen specific TCRs show high affinity docking specific recognition of the particular antigenic polar headgroup, as observable with PG90 and GEM42 TCRs, which contact self-phosphatidylglycerol or foreign glucose monomycolate, respectively (**Figure 6A**) (10, 27).

The BC8B α -chain docks centrally over the F' portal to contact the lipid antigen, and its footprint runs parallel across the antigen binding pocket of CD1b with a lateral escape channel formed by CDR1 α and CDR3 α encompassing the exposed lipid headgroup (**Figure 6B**). As such, TCR α contributes the highest percentage of contacts with the antigenic headgroup, based on buried surface area (BSA) (**Figure 6D**). Of the TCR α CDR loops, it is CDR3 α that coordinates most of the antigenic recognition surface, with BC8B CDR3 α contributing 51% of the total 77% BSA of TCR α against the presented phospholipid antigen. The remainder of the BSA against PI is determined by the framework and CDR3 β residues, which contribute at 7% and 15% of the binding surface, respectively (**Figure 6D**).

In contrast, lipid antigen headgroup recognition is mediated equally by the α - and β - domains of antigen specific TCRs PG90 and GEM42. In both cases, ~50% of TCR docking is mediated by the CDR3 β , which play a role in both antigen headgroup and CD1b contact. Due to differences in PG90 and GEM42 gene usages, as well as differences in antigenic headgroup sizes between PG and GMM, the CDR3 α contact contributions differ amongst these TCRs (**Figure 6D**). Antigen

recognition is dependent on CDR3 α - β centric contacts by PG90 to completely sequester the PG headgroup and anchor onto CD1b, while the GEM42 TCR relies more heavily on the CDR1 β for antigenic anchoring (**Figure 6C-D**).

CD1b-reactive TCRs mediate antigen plasticity within the CD1b binding groove

Remodelling of the lipids within the CD1b binding pocket by TCR CDR is required to accommodate the final docking position and optimal antigen recognition. While the molecular mechanisms of broad and specific antigen recognition differ, antigenic rearrangement is consistently observable across all four CD1b-TCR crystal structures, resulting in partial elevation of the lipid from within the antigen binding groove (**Figure 7**).

While complementary determining region rearrangement is minimal upon docking by the BC8B TCR, the seated antigen's position is elevated 3.6 - 4.0 Å within the A' and C' pockets. Furthermore, the CD1b α 2 hinge region is stabilised and rotated inwards upon BC8B docking (**Figure 7A-B**). In contrast to this antigen lift mechanism, both the PG90 and GEM42 TCRs push the antigenic headgroup towards the F' pocket of CD1b by 4.3 – 6.1 Å, a shift that is accompanied by the CDR3 β surrounding and sequestering the headgroup (10, 27) (**Figure 7C-D**). In all four cases, TCR induced remodelling moves the apparent terminus of the antigenic lipid by ~6-8 Å within the A' pocket, a change which is offset by the change in density corresponding to the bound scaffold lipids in the T' pocket, so that unliganded space within the cleft does not appear. This shift maintains the CD1b-lipid hydrophobic network for binding groove architectural integrity at the base of the A' pocket, despite the variable positioning of bound lipids (**Figure 7**). This comparison demonstrates the plasticity of

lipid placement within the antigen binding pocket of CD1b, and that antigenic remodelling by the TCR is required for energetically optimized binding.

DISCUSSION

Our understanding of CD1-lipid mediated antigen recognition was originally derived from ternary crystal structures of NKT TCRs docking onto CD1d and hexosyl ceramides, whereby the TCR specifically recognises CD1d and the hexose unit of the glycolipid (17, 49, 50). As this general model is expanded to amphipathic ligands other than glycolipids, as well as CD1 isoforms other than CD1d, additional chemical and structural features of TCR interaction with lipid antigens are emerging. TCRs can show extreme specificity for individual head groups (41,51), partial specificity for certain broad classes of lipids (26) or extreme ligand promiscuity for nearly all carried lipids (22, 23). As only the fourth solved ternary structure of a CD1b-lipid-TCR complex, our work structurally validates a mechanism for TCR contact the shared neck regions common to many phospholipids, which occurs through escape of chemically diverse headgroups through a channel in the TCR. Further our data point to unexpected roles of scaffold lipid both in TCR contact and accommodating antigen movement within the cleft, as well as the beginnings of conserved approach angles and TCR footprint positions on CD1b.

Here we show that BC8B CDR3 β contacts both exogenously loaded antigen and reaches down toward the F' portal to contact the endogenous scaffold lipid. Somewhat similar contacts of the CD1c autoreactive $\alpha\beta$ TCR, 3C8, to the spacer lipid have been seen (23), however the CD1b mechanism seen here is different in the sense that the TCR contacts both the spacer and the antigenic lipid. Our data

inform and expand the hypothesis of Camacho, et al., who proposed in context of *M. tuberculosis* sulfoglycolipid recognition, longer chain endogenous scaffold lipids (>C36) could possibly protrude beyond Tyr151 through the F' portal, potentially allowing for antigenic headgroup and scaffold lipid co-contact by the complementarity determining region 3 of the TCR (9). While the long scaffold lipid observed here matched a length of 36 carbons based on electron density, the scaffold does not protrude from the F' portal and instead, the TCR contact inside CD1b is demonstrated directly.

While the function of CD1b-phospholipid reactive $\alpha\beta$ T cells is being elucidated in autoimmunity, the roles of self-reactive T cell such as BC8B is just beginning to be investigated. Further, activation of CD1b+ autoreactive T cells upon phospholipid presentation leads to hyperlipidaemia in mice, indicating a further role of CD1b in autoimmune skin disease (46, 47). Recent transcriptomic analysis revealed that CD1b gene upregulation indicates a positive prognostic score in localised prostate cancer patients (52). Furthermore, there is a marked increase in atypical mixed acyl tail PI species in prostate cancer tissue compared to benign epithelial tissue, which may act as both a potential biomarker for cancer prognosis, as well as antigens for CD1b+ T cells (53). Alternatively, in the case of broadly reactive T cells such as BC8B which do not selectively activate against a specific antigen, these T cells may play a role more in CD1b+ T cell negative thymic selection, with CD1b+ T cells that dock via the antigen specific model of co-recognition playing a direct role in immunity (26).

Altogether, we have provided the molecular mechanisms of self-glycophospholipid presentation by CD1b

and $\alpha\beta$ TCR recognition, expanded on our understanding of the molecular mechanisms CD1b-restricted $\alpha\beta$ TCR autoreactivity. Conceptually, these data contribute to the gradually expanding structural characterisation of TCR recognition of CD1b in defining distinct models of binding, with implications for the direct role of the endogenous scaffold lipid in T cell mediated immune activation. Future alanine scanning mutagenesis studies on TCR interface residues would be of benefit to further characterise mechanisms of docking onto CD1b. The next challenge would be to characterise the functional role autoreactivity mediated by CD1b reactive T cells, and how these self-antigens mediated autoimmune responses in adaptive immunity.

EXPERIMENTAL PROCEDURES

Lipids

Phosphatidylinositol (PI, #850142; C16:0/18:1) was purchased from Avanti® polar lipids. Lyso-sulfatide (lyso, #1904) was purchased from Matreya, LLC.

BC8B and CD1b protein production

Recombinant TCR BC8B was expressed and purified as previously described (26). Briefly, soluble domains of BC8B α and BC8B β were cloned into the pET30a vector, and expressed and refolded via *Escherichia coli* inclusion bodies, then purified by size exclusion chromatography and HiTrap-Q HP anion exchange chromatography to homogeneity. CD1b wild type and alanine scanned mutants were solubly expressed in either *Trichoplusia ni*. High Five insect cell line via baculovirus pFastBac dual transfection, or via the mammalian adherent expression system using Human Embryonic Kidney (HEK) 293 S GnT1-. Soluble CD1b were purified to homogeneity by Ni²⁺-metal affinity chromatography to select for the N terminal hexahistidine tag, followed by size

exclusion chromatography. Purity of BC8B and CD1b were assessed by SDS-PAGE.

Exogenous lipid loading into CD1b

Homogeneity of CD1b-lipid presentation was achieved by loading CD1b with via a two-stage loading protocol previously described (26). Briefly, CD1b was incubated with a molar excess of lysosulfatide at pH = 4.0 and 0.5 % tyloxapol (Merck, #25301-02-4) at room temperature overnight followed by incubation at 37 °C for 60 mins prior to purification via anion exchange chromatography. This was repeated using the CD1b-lysosulfatide sample with PI in a molar excess to obtain a homogeneous sample of CD1b-PI-C34:1. Lipid loading was validated by 4-6.5 pI gradient isoelectric focusing gel (IEF; Cytiva) and anion exchange chromatography. Proteins were buffer exchanged into 10 mM Tris pH 8.0, 150 mM NaCl for crystallographic and biophysical experiments.

Crystallisation and structural determination

Crystals of CD1b-PI-C34:1 and CD1b-PI-C34:1-BC8B were grown via the hanging drop vapour diffusion method at 20 °C. Protein samples were concentrated to 5 mg.mL⁻¹ and mixed with mother liquor at a ratio of 1:1, with a crystallisation condition 24 % (w/v) PEG 3350, 2 % ethylene glycol, 0.2 M Na Iodide for CD1b-PI-C34:1, and 24 % (w/v) PEG 4000, 0.02 M Tris-HCl (pH 7.0), 2 % ethylene glycol for CD1b-PI-C34:1-BC8B. Crystals of CD1b-PI-C34:1 and CD1b-PI-C34:1-BC8B were soaked in a cryoprotectant of 10 % (v/v) ethylene glycol + mother liquor and flash frozen in liquid nitrogen. Data were collected at the Australian Synchrotron at the MX2 beamline and made use of the Australian Cancer Research Foundation EIGER X 16 M detector (DECTRIS) and Synchrotron Blu-Ice software v.1.0 (54). Data were

processed using XDS and scaled using AIMLESS as part of the CCP4i program suite (55). One complete dataset for each complex were collected. Crystal structures were solved by molecular replacement via Phaser as part of the Phenix program suite (56), with CD1b-PC (PDB ID 6D64) and CD1b-PC-BC8B (PDB ID: 6CUG) used as models for CD1b-PI-C34:1 and CD1b-PI-C34:1-BC8B respectively (26). Manual adjustment of each model was conducted in Coot (57), followed by maximum-likelihood refinement with Phenix-refine (56). Molecular representations of structures have been constructed using PyMOL, contacts identified using the CONTACT program, and the centre of mass (C.O.M) calculated using Areaimol within the CCP4i suite (55). Contact distance cut-offs were defined as 3.5 Å for hydrogen bonds, 4.5 Å for salt bridges, and 4.0 Å for Van der Waals (VDW) interactions.

Surface Plasmon Resonance

Surface Plasmon Resonance (SPR) steady state affinity measurements of BC8B against CD1b mutants V72A, R79A, E80A, D83A, Y151A, Q152A, I154A, E156A containing endogenous lipids was conducted at 25 °C on the BIAcore 3000 instrument in 10 mM Tris-HCl (pH 8) and

150 mM NaCl supplemented with 0.5 % (w/v) bovine serum albumen (BSA). 3000 RU of each monomer was coupled on the SA chip, with MHC class-I molecule H-2Db used for reference subtraction. Experiments were conducted as n=2 with two technical duplicates. Steady state affinity calculations using the 1:1 Langmuir binding model, data analysis, and visualization were generated using Graphpad 7.0.

DATA AVAILABILITY

The crystallographic datasets generated and analysed within the current study were deposited to the Protein Data Bank under codes 8DV3 (Crystal structure of CD1b presenting phosphatidylinositol-C34:1) and 8DV4 (Crystal structure of CD1b presenting phosphatidylinositol-C34:1 to $\alpha\beta$ TCR BC8B).

SUPPORTING INFORMATION

This article contains supporting information:

Supplementary Figure 1: Comparison of TCR CDR Leucine binding within the CD1 F' pocket

Supplementary Table 1 Contacts between the BC8B TCR and CD1b-PI

AUTHOR CONTRIBUTIONS

The TCR was cloned and provided by IVR and DBM. Protein expression, lipid loading, x-ray crystallographic and biophysical studies were designed, conducted, and analysed by R.F and A.S. The study was conceived and initiated by AS, with oversight from I.V.R, D.B.M, and J.R. The manuscript was written by R.F, A.S, and J.R and edited by all authors.

FUNDING AND ACKNOWLEDGEMENTS

A. S. Is supported by an Australian ARC DECRA Fellowship (DE210101031); J. R. is supported by an NHMRC Investigator Grant (2008981); D. B. M. is supported by National Institutes of Health grant (R01 AI049313, R01 AR048632).

CONFLICT OF INTEREST

The authors declare that they have no conflicts of interest. DBM consults for Enara and Pfizer.

REFERENCES

1. Moody D, Ulrichs T, Mühlecker W, Young DC, Gurcha SS, Grant E, Rosat JP, Brenner MB, Costello CE, Besra GS, Porcelli SA. (2000) CD1c-mediated T-cell recognition of isoprenoid glycolipids in *Mycobacterium tuberculosis* infection. *Nature* **404**(6780), 884-888
2. Ulrichs T, Moody DB, Grant E, Kaufmann SH, Porcelli SA. (2003) T-cell responses to CD1-presented lipid antigens in humans with *Mycobacterium tuberculosis* infection. *Infection and immunity* **71**(6), 3076-3087
3. Van Rhijn I, Young DC, De Jong A, Vazquez J, Cheng TY, Talekar R, Barral DC, León L, Brenner MB, Katz JT, Riese R, Ruprecht RM, O'Conner PB, Costello CE, Porcelli SA, Briken V, Moody DB. (2009) CD1c bypasses lysosomes to present a lipopeptide antigen with 12 amino acids. *Journal of Experimental Medicine* **206**(6), 1409-1422
4. Zajonc DM, Crispin MDM, Bowden TA, Young DC, Cheng TY, Hu J, Costello CE, Rudd PM, Dwek RA, Miller MJ, Brenner MB, Moody DB, Wilson IA. (2005) Molecular mechanism of lipopeptide presentation by CD1a. *Immunity* **22**(2), 209-219
5. Moody DB, Young DC, Cheng TY, Rosat JP, Roura-Mir C, O'Connor PB, Zajonc DM, Walz A, Miller MJ, Levery SB, Wilson IA, Costello CE, Brenner MB. (2004) T cell activation by lipopeptide antigens. *Science* **303**(3), 222-229
6. Matsunaga I, Sugita M. (2012) Mycoketide: a CD1c-presented antigen with important implications in mycobacterial infection. *Clinical and Developmental Immunology*. **981821**, 1-7
7. Scharf L, Nan-Shen L, Hawk AJ, Garzón D, Zhang T, Fox LM, Kazen AR, Shah S, Haddadian EJ, Gumperz JE, Saghatelian A, Garaldo-Gómez JD, Meredith SC, Piccirilli JA, Adams EJ. (2010) The 2.5 Å structure of CD1c in complex with a mycobacterial lipid reveals an open groove ideally suited for diverse antigen presentation. *Immunity* **33**(6), 853-862
8. Beckman EM, Melián A, Behar SM, Sieling PA, Chatterjee D, Furlong ST, Matsumoto R, Rosat JP, Modlin RL, Porcelli SA. (1996) CD1c restricts responses of mycobacteria-specific T cells. Evidence for antigen presentation by a second member of the human CD1 family. *The Journal of Immunology*. **157**(7), 2795-2803
9. Camacho F, Moreno E, Garcia-Alles LF, Chinea Santiago G, Gilleron M, Vasquez A, Choong YS, Reyes F, Norazmi MN, Sarmiento ME, Acosta A. (2020) A Direct Role for the CD1b Endogenous Spacer in the Recognition of a *Mycobacterium tuberculosis* Antigen by T-Cell Receptors. *Frontiers in Immunology*. **11**, 566710
10. Gras S, Van Rhijn I, Shahine A, Cheng TY, Bhati M, Tan LL, Halim H, Tuttle KD, Gapin L, Le Nours J, Moody DB, Rossjohn J. (2016) T cell receptor recognition of CD1b presenting a mycobacterial glycolipid. *Nature Communications* **7**, 13257
11. Van Rhijn I, Kasmar A, de Jong A, Gras S, Bhati M, Doorenspleet ME, de Vries N, Godfrey DI, Altman JD, de Jager W, Rossjohn J, Moody DB. (2013) A conserved human T cell population targets mycobacterial antigens presented by CD1b. *Nature Immunology* **14**(7), 706-713
12. Batuwangala T, Shepherd D, Gadola SD, Gibson KJC, Zaccari NR, Fersht AR, Besra GS, Cerundolo V, Jones EY. (2004) The Crystal Structure of Human CD1b with a Bound Bacterial Glycolipid. *The Journal of Immunology* **172**(4), 2382-2388

13. Moody DB, Guy MR, Grant E, Cheng TY, Brenner MB, Besra GS, Porcelli SA. (2000) CD1b-mediated T cell recognition of a glycolipid antigen generated from mycobacterial lipid and host carbohydrate during infection. *The Journal of Experimental Medicine*. **192(7)**, 965-976
14. Roy S, Ly D, Li NS, Altman JD, Piccirilli JA, Moody DB, Adams EJ. (2014) Molecular basis of mycobacterial lipid antigen presentation by CD1c and its recognition by $\alpha\beta$ T cells. *Proceedings of the National Academy of Sciences*. **111(43)**, E4648-4657
15. Melum E, Jiang X, Baker KD, Macedo MF, Fritsch J, Dowds CM, Wang J, Pharo A, Kaser A, Tan C, Pereira CS, Kelly SL, Duan J, Karlsen TH, Exley MA, Schütze S, Zajonc DM, Merrill AH, Schuchman EH, Zeissig S, Blumberg RS. (2019) Control of CD1d-restricted antigen presentation and inflammation by sphingomyelin. *Nature Immunology* **20(12)**, 1644-1655
16. Wegrecki M, Ocampo TA, Gunasignhe SD, von Borstel A, Tin SY, Reijneveld JF, Cao TP, Gully BS, Le Nours J, Moody DB, van Rhijn I, Rossjohn J. (2022) Atypical sideways recognition of CD1a by autoreactive $\gamma\delta$ T cell receptors. *Nature communications* **13(1)**, 1-15
17. Borg NA, Wun KS, Kjer-Nielsen L, Wilce MC, Pellicci DG, Koh R, Besra GS, Bharadwaj M, Godfrey DI, McCluskey J, Rossjohn J. (2007) CD1d–lipid-antigen recognition by the semi-invariant NKT T-cell receptor. *Nature* **448(7)**, 44-49
18. Gumperz JE, Roy C, Makowska A, Lum D, Sugita M, Podrebarac T, Yoezuka Y, Porcelli SA, Cardell S, Brenner MB, Behar SM. (2000) Murine CD1d-restricted T cell recognition of cellular lipids. *Immunity* **12(2)**, 211-221
19. Cotton RN, Cheng TY, Wegrecki M, Le Nours J, Orgill DP, Pomahac B, Talbot SG, Willis RA, Altman JD, de Jong A, Ogg G, Van Rhijn I, Rossjohn J, Clark RA, Moody DB. (2021) Human skin is colonized by T cells that recognize CD1a independently of lipid. *The Journal of Clinical Investigation*. **131(1)**, e140706
20. Cotton RN, Wegrecki M., Cheng TY, Chen YL, Veerapen N, Le Nours J, Orgill DP, Pomahac B, Talbot SG, Willis R, Altman JD. (2021) CD1a selectively captures endogenous cellular lipids that broadly block T cell response. *Journal of Experimental Medicine*. **218(7)**, e20202699fG
21. Nicolai S, Wegrecki M., Cheng TY, Bourgeois EA, Cotton RN, Mayfield JA, Monnot GC, Le Nours J, Van Rhijn I, Rossjohn J, Moody DB. (2020) Human T cell response to CD1a and contact dermatitis allergens in botanical extracts and commercial skin care products. *Science Immunology* **5(43)**, eaax5430
22. Birkinshaw RW, Pellici D., Cheng TY, Keller AN, Sandoval-Romero M, Gras S, de Jong A, Uldrich AP, Branch Moody D, Godfrey DI, Rossjohn J. (2015) $\alpha\beta$ T cell antigen receptor recognition of CD1a presenting self lipid ligands. *Nature Immunology* **16(3)**, 258-266
23. Wun KS, Reijneveld JF, Cheng TY, Ladell K, Uldrich AP, Le Nours J, Miners KL, McLaren JE, Grant EJ, Haigh OL, Watkins TS, Suliman S, Iwany S, Jimenez J, Calderon R, Tamara KL, Leon SR, Murray MB, Mayfield JA, Altman JD, Purcell AW, Miles JJ, Godfrey DI, Gras S, Price DA, Van Rhijn I, Moody DB, Rossjohn J. (2018) T cell autoreactivity directed toward CD1c itself rather than toward carried self lipids. *Nature Immunology*. **19(4)**, 397-406
24. Mansour S, Tocheva AS, Cave-Ayland C, Machelett MM, Sander B, Lissin NM, Molloy PE, Baird MS, Stübs G, Schröder NW, Schumann RR. (2016) Cholesteryl esters stabilize human CD1c conformations for recognition by self-reactive T cells. *Proceedings of the National Academy of Sciences* **113(9)**, E1266-1277

25. Reijneveld JF, Ocampo T, Shahine A, Gully BS, Vantourout P, Hayday AC, Rossjohn J, Moody DB, Van Rhijn I. (2020) Human $\gamma\delta$ T cells recognize CD1b by two distinct mechanisms. *Proceedings of the National Academy of Sciences* **117(37)**, 22944-22952
26. Shahine A, Reinink P, Reijneveld J F, Gras S, Holzheimer M, Cheng TY, Minnaard AJ, Altman JD, Lenz S, Prandi J, Kubler-Kielb J, Moody DB, Rossjohn J, Van Rhijn I. (2019) A T-cell receptor escape channel allows broad T-cell response to CD1b and membrane phospholipids. *Nature Communications* **10**: 56
27. Shahine A, van Rhijn I, Cheng TY, Iwany S, Gras S, Moody DB, Rossjohn J. (2017) A molecular basis of human T cell receptor autoreactivity toward self-phospholipids. *Science Immunology* **2(16)**, aao1384
28. Brigl M and Brenner MB. (2004) CD1: Antigen Presentation and T Cell Function. *Annual Review of Immunology* **22**, 817-890
29. Moody DB, Cotton R. (2017) Four pathways of CD1 antigen presentation to T cells. *Current Opinion in Immunology* **46**, 127-133
30. Reijneveld JF, Marino L, Cao TP, Cheng TY, Dam D, Shahine A, Witte MD, Filippov DV, Suliman S, van der Marel GA, Moody DB. (2021) Rational design of a hydrolysis-resistant mycobacterial phosphoglycolipid antigen presented by CD1c to T cells. *Journal of Biological Chemistry* **297(4)**, 101197
31. Patel O, Pellicci DG, Gras S, Sandoval-Romero ML, Uldrich AP, Mallevaey T, Clarke AJ, Le Nours J, Theodossis A, Cardell SL, Gapin L, Godfrey DI, Rossjohn J. (2012) Recognition of CD1d-sulfatide mediated by a type II natural killer T cell antigen receptor. *Nature Immunology* **13**, 857-863
32. Girardi E, Maricic I, Wang J, Mac TT, Iyer P, Kumar V, Zajonc DM. (2012) Type II natural killer T cells use features of both innate-like and conventional T cells to recognize sulfatide self antigens. *Nature Immunology* **13(9)**, 851-856
33. Rossjohn J, Pellicci D, Patel O, Gapin L, Godfrey DI (2012) Recognition of CD1d-restricted antigens by natural killer T cells. *Nature Reviews Immunology* **12(12)**, 845-857
34. Shahine A, Wegrecki M, Le Nours J. (2021) Novel molecular insights into human lipid-mediated T cell immunity. *International Journal of Molecular Sciences*. **22(5)**, 2617
35. Garcia-Alles LF, Verslui K, Maveyraud L, Vallina AT, Sansano S, Bello NF, Guber H J, Guillet V, de la Salle H, Puzo G. (2006) Endogenous phosphatidylcholine and a long spacer ligand stabilize the lipid-binding groove of CD1b. *The EMBO journal* **25(15)**, 3684-3692
36. Gadola SD, Zaccari NR, Harlos K, Shepherd D, Castro-Palomino J C, Ritter G, Schmidt RR, Jones EY, Cerundolo V. (2002) Structure of human CD1b with bound ligands at 2.3 Å, a maze for alkyl chains. *Nature Immunology* **3(8)**, 721-726
37. Garcia-Alles LF, Collmann A, Versluis C, Lindner B, Guiard J, Maveyraud L, Huc E, Im JS, Sansano S, Brando T, Julien S, Prandi J, Gilleron M, Porcelli SA, de la Salle H, Heck AJ, Mori L, Puzo G, Mourey L, De Libero G. (2011) Structural reorganization of the antigen-binding groove of human CD1b for presentation of mycobacterial sulfolipids. *Proceedings of the National Academy of Sciences* **108(43)**, 17755-17760
38. Shahine A. (2018) The intricacies of self-lipid antigen presentation by CD1b. *Molecular Immunology* **104**, 27-36
39. Beckman EM, Porcelli S, Morita CT, Behar SM, Furlong ST, Brenner MB. (1994) Recognition of a lipid antigen by CD1-restricted $\alpha\beta^+$ T cells. *Nature* **372(6705)**, 691-694

40. Layre E, Collmann A, Bastian M, Mariotti S, Czaplicki J, Prandi J, Mori L, Stenger S, De Libero G, Puzo G, Gilleron M. (2009) Mycolic acids constitute a scaffold for mycobacterial lipid antigens stimulating CD1-restricted T cells. *Chemistry & Biology* **16(1)**, 82-92
41. Moody DB, Reinhold BB, Guy MR, Beckman EM, Frederique DE, Furlong ST, Ye S, Reinhold VN, Sieling PA, Modlin RL, Besra GS, Porcelli SA. (1997) Structural requirements for glycolipid antigen recognition by CD1b-restricted T cells. *Science* **278(5336)**, 283-286
42. Reinink P, Shahine A., Gras S, Cheng TY, Farquhar R, Lopez K, Suliman SA, Reijneveld JF, Le Nours J, Tan LL, León SR. (2019) A TCR β -chain motif biases toward recognition of human CD1 proteins. *The Journal of Immunology* **203(12)**, 3395-3406
43. Roura-Mir C, Wang L, Cheng TY, Matsunaga I, Dascher CC, Peng SL, Fenton MJ, Kirschning C, Moody DB. (2005) Mycobacterium tuberculosis regulates CD1 antigen presentation pathways through TLR-2. *The Journal of Immunology*. **175(3)**, 1758-1766
44. Leslie DS, Dascher CC, Cembrola K, Townes MA, Hava DL, Hugendubler LC, Mueller E, Fox L, Roura-Mir C, Moody DB, Vincent MS. (2008) Serum lipids regulate dendritic cell CD1 expression and function. *Immunology* **125(3)**, 289-301
45. Van Rhijn I, van Berlo T, Hilmenyuk T, Cheng TY, Wolf BJ, Tatituri RV, Uldrich AP, Napolitani G, Cerundolo V, Altman JD, Willemsen P. (2016) Human autoreactive T cells recognize CD1b and phospholipids. *Proceedings of the National Academy of Sciences*. **113**, 380-385
46. Bagchi S, He Y, Zhang H, Cao L, Van Rhijn I, Moody DB, Gudjonsson JE, Wang C-R. (2017) CD1b-autoreactive T cells contribute to hyperlipidemia-induced skin inflammation in mice. *The Journal of Clinical Investigation* **127(6)**, 2339-2352
47. Bagchi S, Li S, Wang C-R. (2016) CD1b-autoreactive T cells recognize phospholipid antigens and contribute to antitumor immunity against a CD1b(+) T cell lymphoma. *Oncoimmunology* **5(9)**, e1213932
48. Gras S, van Rhijn I, Shahine A, Le Nours J. (2018) Molecular recognition of microbial lipid-based antigens by T cells. *Cellular and Molecular Life Sciences* **75(9)**, 1623-1639
49. Cotton RN, Shahine A, Rossjohn J, Moody DB. (2018) Lipids hide or step aside for CD1-autoreactive T cell receptors. *Current Opinion in Immunology* **52**, 93-99
50. Rossjohn J, Gras S, Miles JJ, Turner SJ, Godfrey DI, McCluskey J. (2015) T cell antigen receptor recognition of antigen-presenting molecules. *Annual Review of Immunology* **33**, 169-200
51. Kawano T, Cui J, Yoezuka Y, Toura I, Kaneko Y, Motoki K, Ueno H, Nakagawa R, Sato H, Kondo E, Koseki H, Taniguchi M. (1997) CD1d-restricted and TCR-mediated activation of valpha14 NKT cells by glycosylceramides. *Science* **278(5343)**:1626-1629
52. Lee CH, Chen LC, Yu CC, Lin WH, Lin VC, Huang CY, Lu TL, Huang SP, Bao BY. (2019) Prognostic value of CD1B in localised prostate cancer. *International journal of environmental research and public health* **16(23)**, 4723-4832
53. Goto T, Terada N, Inoue T, Nakayama K, Okada Y, Yoshikawa T, Miyazaki Y, Uegaki M, Sumiyoshi S, Kobayashi T, Kamba T. (2014) The expression profile of phosphatidylinositol in high spatial resolution imaging mass spectrometry as a potential biomarker for prostate cancer. *Plos One* **9(2)**, e90242
54. Aragão D, Aishima J, Cherukuvada H, Clarken R, Clift M, Cowieson NP, Ericsson DJ, Gee CL, Macedo S, Mudie N, Panjekar S, Price JR, Riboldi-Tunnicliffe A, Rostan R, Williamson R, Caradoc-Davies TT. (2018) MX2: a high-flux undulator microfocus beamline serving

- both the chemical and macromolecular crystallography communities at the Australian Synchrotron. *Journal of Synchrotron Radiation* **25(3)**, 885-891
55. Winn MD BC, Cowtan KD, Dodson EJ, Emsley P, Evans PR, Keegan RM, Krissinel EB, Leslie AG, McCoy A, McNicholas SJ. (2011) Overview of the CCP4 suite and current developments. *Acta Crystallographica Section D: Biological Crystallography* **67(4)**, 235-242
56. Adams PD, Afonine PV, Bunkóczi G, Chen VB, Davis IW, Echols N, Headd JJ, Hung LW, Kapral GJ, Grosse-Kunstleve RW, McCoy AJ. (2010) PHENIX: a comprehensive Python-based system for macromolecular structure solution. *Acta Crystallographica Section D: Biological Crystallography* **66(2)**, 212-212
57. Emsley P, Lohkamp B, Scott WG, Cowtan K. (2010) Features and development of Coot. *Acta Crystallographica Section D: Biological Crystallography* **66(4)**, 486-501

FIGURE LEGENDS

Figure 1. CD1b lipid loading validation. **A.** Anion exchange chromatographs show CD1b treated with 0.5 % tyloxapol (mock), CD1b loaded with lysosulfatide, and CD1b loaded with phosphatidylinositol (PI). The dashed line indicates peak elution at gradient level (mS/cm²). **B.** Isoelectric focusing (IEF) analysis validated successful lipid loading of PI-C34:1 by CD1b. The IEF gel of CD1b shows complexes containing endogenous (endo) lipids, detergent treated CD1b (mock), CD1b presenting lysosulfatide (L-SF), and CD1b presenting PI-C34:1 (PI). Lipid loading success was determined by charge separation of each protein on the gel. Migration of CD1b-PI-C34:1 protein towards the negative anode (-) and indicates successful loading of the lipid of interest in comparison to CD1b presenting endogenous lipids and CD1b presenting lysosulfatide.

Figure 2. Presentation of PI-C34:1 by CD1b and comparison with refolded CD1b-PI-C33:0. **A.** Structural overview of CD1b (grey), β 2m (black) presenting bound phosphatidylinositol C34:1 PI-C34:1, yellow) and scaffold wax ester lipid (purple) within the antigen binding cleft. **B.** CD1b-PI-C34:1 binary crystal structure unbiased (green, upper) and refined (blue, lower) electron density maps of PI and scaffold lipids bound within the CD1b antigen binding pocket. Unbiased and refined maps are contoured to 2.5 σ and 0.8 σ respectively. **C-D.** Structural comparison overlay between the binding clefts of CD1b presenting PI-C34:1 (CD1b-PI-C34:1, yellow) and refolded CD1b-PI-C33:0 (PDB ID: 1GZP, green), with a focus on **C.** the phospholipid antigen headgroups around the α 2 helix hinge region, and **D.** The buried F' pocket and overlay between scaffold (pink) and detergent (purple) molecules. Amino acids are represented as sticks, with directions of movement indicated by black arrows. Nitrogen, oxygen, and sulfur atoms are coloured in blue, red, and orange respectively.

Figure 3. Overview of presentation of PI-C34:1 by CD1b to BC8B TCR and comparison with unliganded CD1b-PI-C34:1. **A.** Ribbon diagram overview of CD1b (grey), β 2m (black) presenting PI-C34:1 (light orange) and scaffold lipid (purple), and BC8B TCR (α -chain blue, β -chain green). Dashed lines on BC8B TCR α -chain is as indicate missing residues not visible in the electron density. **B.** CD1b-PI-C34:1-BC8B TCR ternary crystal structure unbiased (green, upper) and refined (blue, lower) electron density maps of PI and scaffold lipids bound within the CD1b antigen binding pocket. Unbiased and refined maps are contoured to 2.5 σ and 0.8 σ respectively. **C.** Comparison of presentation of PI-C34:1 in the unliganded CD1b-PI-C34:1 (yellow) and CD1b-PI-C34:1-BC8B (orange) crystal structures. Arrow indicates upward directional movement of the PI antigen headgroup upon BC8B TCR docking. Oxygen and sulfur atoms are coloured in red and orange, respectively.

Figure 4. BC8B TCR recognition of PI-C34:1 and CD1b. **A.** BC8B TCR α -chain Framework (FW α), CDR1 α (teal) and CDR3 α (purple), as well as the CDR3 β of BC8B TCR β -chain, contact the headgroup and neck region of PI-C34:1 via H-bonds (black dashed lines). Residues involved in lipid contacts are represented as sticks. **B.** Comparison of lipid presentation in the ternary complexes CD1b-PC-BC8B (PDB ID: 6CUG) and CD1b-PI-C34:1-BC8B indicate that the escape channel (labelled) formed between the CDR1 α (teal) and CDR3 α (purple) by docking of BC8B on top of CD1b-lipid remains intact, and the escape channel diameter is conserved (black dashed line). Neck regions and phosphate groups of PC (blue) and PI-C34:1 (light

orange) overlay directly and both headgroups are accommodated. **C.** TCR CDR3 α and CDR3 β facilitate key contacts with CD1b along the CD1b α 1 region (grey). **D.** Leu111 β of the BC8B TCR β -chain (yellow) contacts both the PI-C34:1 and scaffold lipid simultaneously via hydrophobic interactions (green dashed lines). Black arrows between CD1b-PI-C34:1 before (blue) and after (grey) BC8B TCR binding indicate direction of movement.

Figure 5. Surface plasmon resonance (SPR) steady state affinities of BC8B interacting with CD1b alanine mutants of surface amino acids. **A.** BC8B binding against wild type CD1b (CD1b-WT) alanine mutants were determined to establish the functional contact sites of the BC8B TCR and compared to interaction sites determined from structural studies. SPR experiments were conducted with 2 independent measurements in technical replicates, and steady state (K_D) measurements with error bars representing standard error of the mean (SEM) are shown. GraphPad Prism Software was used to generate sensorgrams (upper panel) and equilibrium curves (lower panel). **B.** The surface representation of CD1b (grey surface) with mutants was colour-coded based on the effect on binding affinity of the BC8B TCR: dark grey had no effect; yellow had less than 3-fold reduction; orange had between 3 to 5-fold reduction; red indicates greater than 5-fold reduction. **C-D.** Mutated residues are colour coded as 5B. Black dashes represent hydrogen bond formation. TCR CDR3 α , CDR1 β , and CDR3 β are coloured in purple, teal, and yellow respectively. Lipids PI and scaffold are coloured in light orange and purple respectively. Oxygen, nitrogen, and sulfur are coloured red, blue, and orange respectively.

Figure 6. Comparison of CD1b-PI-C34:1-BC8B with ternary structures of CD1b-lipid complexes. **A.** Ribbon diagrams of ternary complexes of CD1b presenting self (CD1b-PI-C34:1-BC8B, CD1b-PC-C34:1-BC8B, CD1b-PG-PG90) and foreign lipids (CD1b-GMM-GEM42) for $\alpha\beta$ -TCR recognition. The BC8B TCR escape channels formed between the CDR1 α and CDR3 α are highlighted **B.** Spheres colour coded to the respective α chain and β chains of the respective TCR complex representing the centre of mass of the TCR. CD1b-PI-C34:1-BC8B (α -chain blue, β -chain green), CD1b-GMM-GEM42 (α -chain brown, β -chain pale pink), CD1b-PG-PG90 (α -chain orange, β -chain pale blue) **C.** $\alpha\beta$ -TCR contacts of lipid antigens presented by CD1b. CDR1 α (teal), CDR3 α (purple), CDR2 β (green), and CDR3 β (yellow) directly involved in lipid antigen recognition are represented as ribbons, with contact residues as sticks, and H-bonds (black dashed lines) with exposed head and neck regions of antigenic lipids. **D.** Pie chart graphical representation of percentage buried surface area (%) between antigenic lipid headgroup and TCR framework (blue), CDR1 α (teal), CDR2 α (green), CDR3 α (purple), CDR1 β (red), and CDR3 β (yellow).

Figure 7. Comparison of lipid reorganisation within the CD1b binding groove upon TCR docking. Side view structural overlays of CD1b-lipid binary complexes (light) and CD1b-TCR complexes (dark) of **A.** CD1b-PI-32:1-BC8B (yellow), **B.** CD1b-PC-BC8B (red), **C.** CD1b-PG-PG90 (green), and **D.** CD1b-GMM-GEM42 (blue). CD1b α 1 and α 2 helices (grey), as well as TCR CDR3 α (purple) and CDR3 β (yellow) are represented as surfaces (upper) and ribbons (lower), with lipid antigens and scaffold lipids represented as sticks. Arrows indicate direction and distance (in Å) of movement for CD1b (black), TCR (red), antigenic lipid (blue), and scaffold lipid (green).

Supplementary Figure 1: Comparison of TCR CDR Leucine binding within the F' pockets of CD1 molecules. Leu111 β of the BC8B TCR β -chain (yellow) contacts bound lipids and Phe84

of CD1b (grey) upon **A.** PI (wheat) and **B.** PC (blue), as well as endogenous scaffold lipid (purple) presentation. In comparison, **C.** Leu110 β of the GEM42 TCR in complex with CD1b presenting glucose monomycolate (GMM, orange), and **D.** Leu99 α of NKT15 iNKT TCR in contact with human CD1d (light blue) presenting α -galactosylceramide (α GalCer, red) in turn favour hydrophobic contacts (green dash) with Phe84 within the CD1 F' pocket.

Table 1: X-ray data collection and refinement statistics

	CD1b-PI	BC8B-CD1b-PI
Space Group	P 21 21 21	P 1 21 1
Resolution Range (Å)	46.39 – 1.90 (1.97-1.90)	41.13 – 2.40 (2.49-2.40)
Cell Dimensions (Å, °)	a=57.82, b=78.63, c=92.73 $\alpha=\beta=\gamma$ 90	a=73.09, b=65.43, c=101.58 $\alpha=\gamma=90$ $\beta=102.26$
Total no. of reflections	496450 (31344)	260716 (26509)
No. of unique reflections	33822 (3316)	36933 (3651)
Multiplicity	14.70 (14.70)	7.10 (6.90)
Completeness (%)	99.32 (98.66)	99.88 (99.86)
CC (1/2)	0.99 (0.73)	0.99 (0.87)
R_{pim} (%) ^a	6.20 (63.50)	5.90 (58.80)
Mean $I/\sigma(I)$ ^b	13.50 (2.10)	11.60 (2.20)
$R_{\text{factor}}/R_{\text{free}}$ (%) ^c	18.70 / 24.54	19.06 / 24.89
Non-hydrogen atoms	3585	6746
Macromolecules	3042	6247
Ligand	242	251
Solvent	301	248
Protein Residues	380	821
Bond Length (Å)	0.011	0.011
Bond Angles (°)	1.22	1.27
Ramachandran Plot		
Favoured Region (%)	98.94	97.10
Allowed Region (%)	1.03	2.90
Outliers (%)	0.00	0.00
B-Factors (Å²)		
Average B-factors	33.41	61.12
Macromolecules	31.14	61.94
Ligands	54.81	81.40
Solvent	39.20	58.11
PDB ID	8DV3	8DV4

$$^a R_{\text{pim}} = \sum_{\text{hkl}} [1/(N-1)]^{1/2} \sum_i |I_{\text{hkl},i} - \langle I_{\text{hkl}} \rangle| / \sum_{\text{hkl}} \langle I_{\text{hkl}} \rangle,$$

^b $\sigma(I)$ is the estimated standard deviation of the integrated intensity (I).

$$^c R_{\text{factor}} = \sum_{\text{hkl}} ||F_{\text{O}}| - |F_{\text{C}}|| / \sum_{\text{hkl}} |F_{\text{O}}| \text{ for all data except 5\%, which were used for } R_{\text{free}} \text{ calculation.}$$

Highest resolution shell is shown in parenthesis.

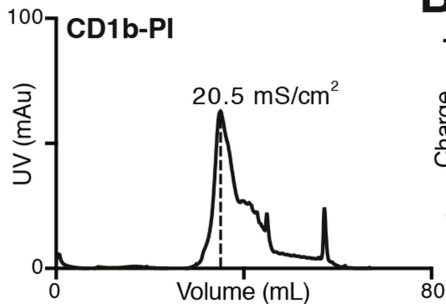
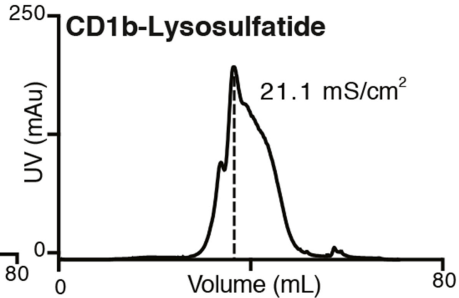
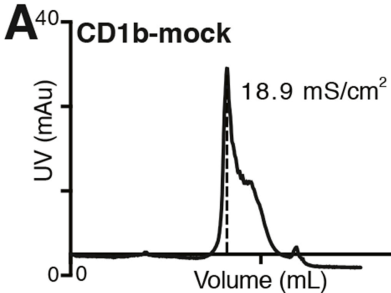
CONFLICT OF INTEREST

The authors declare that they have no conflicts of interest. DBM consults for Enara and Pfizer.

Journal Pre-proof

Author contributions

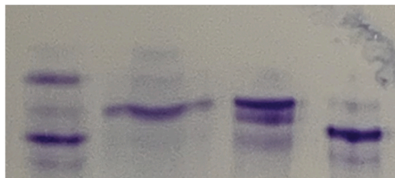
The TCR was cloned and provided by IVR and DBM. Protein expression, lipid loading, x-ray crystallographic and biophysical studies were designed, conducted, and analysed by R.F and A.S. The study was conceived and initiated by AS, with oversight from I.V.R, D.B.M, and J.R. The manuscript was written by R.F, A.S, and J.R and edited by all authors.



B

+

Charge



Endo

Mock

L-SF

PI

